Science
AAAS

Supplementary Materials for

Dynamic interplay between metal nanoparticles and oxide support under redox conditions

H. Frey *et al*.

Corresponding authors: X. Huang, xinghuang@fzu.edu.cn; J. A. van Bokhoven, jeroen.vanbokhoven@chem.ethz.ch; M. G. Willinger, marc.willinger@tum.de

Science **376**, 982 (2022)
DOI: 10.1126/science.abm3371

The PDF file includes:

Materials and Methods
Figs. S1 to S6
References

Other Supplementary Material for this manuscript includes the following:

Movies S1 to S8

Materials and Methods

Synthesis

The catalyst was prepared by incipient wetness impregnation of a titanium (IV) oxide support (Aeroxide® P25, Acros Organics) with tetraammineplatinum (II) nitrate (99.995 %, Sigma Aldrich) dissolved in ultrapure MilliQ® water. After calcination at 200 °C in static air for 5 h (heating rate: 10 °C min^{-1}), the catalyst with a platinum weight loading of 2% was transferred into a quartz tube and heated under He flow (50 mL min^{-1}) in a tubular oven to 700 °C for 1 h (heating rate: 10 °C min^{-1}). Subsequent XRD measurements showed no signs of anatase phase after calcination. A detailed synthesis protocol can be found elsewhere (5).

In situ TEM

In situ TEM studies were performed using the aberration-corrected 300 kV JEOL Grand-ARM300F of the Scientific Center of Optical and Electron Microscopy (ScopeM) at ETH Zürich. A DENSsolutions Climate+ System was used to study samples under controlled gas-flow, pressure and temperature conditions. The setup was coupled to a quadrupole mass spectrometer (MS) (JEOL, JMS-TQ4000GC), for simultaneous detection of catalytic conversion. For additional experiments, the quadrupole mass spectrometer was exchanged with a (RC PIC Quadrupole Mass Spectrometer, Hiden Analytical). After dispersion in chloroform and ultrasonication for 30 minutes, sample material was drop-deposited onto the heating chip, and then mounted onto the DENSsolutions Climate holder. After leak-testing and insertion of the holder in the microscope, the samples were exposed to oxygen for 30 minutes at 300 °C in order to remove residual carbon contamination (po_2 = 200 mbar). This cleaning procedure prevents the building up of carbon deposits during subsequent electron beam imaging. In order to make sure that the observed changes were not caused by electron beam irradiation, we adjusted the illumination conditions throughout

the experiments such that the electron beam dose rate was below the threshold electron dose determined by Kuwauchi *et al.* (*36*) (~ $1x10^4$ e^- $Å^{-2}s^{-1}$). We furthermore compared regions that were exposed to the beam during gas-phase switching with other, non-exposed regions. Since all observed particles showed identical encapsulation (and reproducible behavior in multiple experiments), we can safely conclude that the state of the particles and overgrowth layer are not due to electron beam irradiation.

Protocol

Pretreatment

After the cleaning procedure, oxygen was removed from the gas mixture and the sample was exposed to a reductive treatment in order to induce a classical SMSI state (3,4,32). The pretreatment consisted of a heating step to 600 °C in helium followed by exposure to hydrogen (p_{H2} = 700 mbar) for 60 minutes.

The final step of the pretreatment consisted of flushing out hydrogen with helium that was subsequently replaced by oxygen (p_{O2} = 700 mbar) in order to prepare the system for the study of redox catalysis under oxygen rich conditions.

Initiation of the classical SMSI state

The initial Pt/TiO_2 (2 weight % of Pt) contained Pt particles of various shapes in the size range between 2 and 20 nm. Amongst them, the most representative particles were about 10-15 nm in size and shaped in the form of a truncated cuboctahedron, exposing mostly {111} and {100} facets (see Fig. **S1 A-C**). The starting point of our investigation was the classical SMSI state, which was induced by heating the catalyst to 600 °C in a flow of hydrogen at 700 mbar inside the TEM using a DENSsolutions Climate holder. This in situ reductive activation results in the typical

encapsulation of Pt particles by a thin, partially reduced layer of TiO_2 (5–9). Once this classical SMSI state was established (**Fig. S1 D**), the gas phase was switched in steps, first from reducing conditions to inert He, then to pure O_2 and finally, to an oxygen-rich, reactive H_2+O_2 mixture. During the gas-switching, the sample temperature and total pressure were kept constant at 600 °C and 760 mbar, respectively.

Switching to oxygen atmosphere

No structural changes were observed during the gradual replacement of hydrogen by helium (**Fig. S2**). After hydrogen was fully flushed out of the reactor, O_2 was introduced. The switching from inert to oxidizing conditions did not show any obvious effect on the particle shape but resulted in a change of the overlayer structure (panels **D** and **E** in **Fig. S1**). It gained in thickness and developed a particular double-layered arrangement. The swelling of the overlayer and the frequently observed formation of patches of excess material (see arrows in **Fig. S1 F** & **Fig. S2 C**) are indicative of a re-oxidation of the initial SMSI overlayer, possibly with contributions from de-alloying of a platinum-titanium alloy that formed at the particle surface during high-temperature reduction (*5*). **Fig. S1 E** shows how the configuration of the overlayer under oxygen depends on the surface structure of the Pt NPs: ordered structures form on the {111} facets, and ill-structured, amorphous titania exist on the {100} planes and {110} microfacets as well as kinks and edges between these facets. Ordered low-energy configurations can only form on facets where the structural incoherence between possible crystalline configurations of the overlayer and the platinum surface and thus, the interfacial energy, is low (*75*). Since the structures of the overlayer and the composition of the interface depend on the chemical environment, an integral description of SMSI layers, especially on the basis of ex situ observations, is insufficient. This becomes even

more evident in the next step, when we describe the observations made upon switching from oxidizing conditions to the reactive redox regime.

Reaction conditions

After 30 minutes, a small amount of H_2 (p_{H2} = 60 mbar) was added to the oxygen flow. The O_2 partial pressure was held constant over the course of the experiment. When H_2 was retracted from the gas mixture, the resulting partial pressure loss was compensated by adding the same amount of helium to the system.

Water addition

Additional experiments were performed in order to elucidate the influence of water on the observed dynamics. To saturate the feed gas flow with water vapor, a capillary humidifier was designed and integrated into the gas-feeding system of the *in situ* TEM set-up. The saturator consists of a P80 polypropylene tubular membrane (Zena-Membranes) that is submerged in degassed ultrapure water and sealed against surrounding atmosphere. The pore size and the hydrophobic character of the membrane prevent water diffusion into the inside lumen of the membrane but allow for water vapor transport. The theoretical upper limit for the water vapor partial pressure in the system was calculated based on the saturation vapor pressure of water at 23°C and the relatively lower pressure in the nanoreactor (1000 mbar) with respect to that of the humidifier (1414 mbar) that is situated upstream the nanoreactor. For our experiments, the maximal excess water vapor that could be added was 19.8 mbar. Note that due to the replacement of a defective mass-flow-controller, the hydrogen flow required to enter the redox regime differed slightly from previous experiments (set value of x_{H2} = 0.14 instead of 0.08).

Fig. S1.

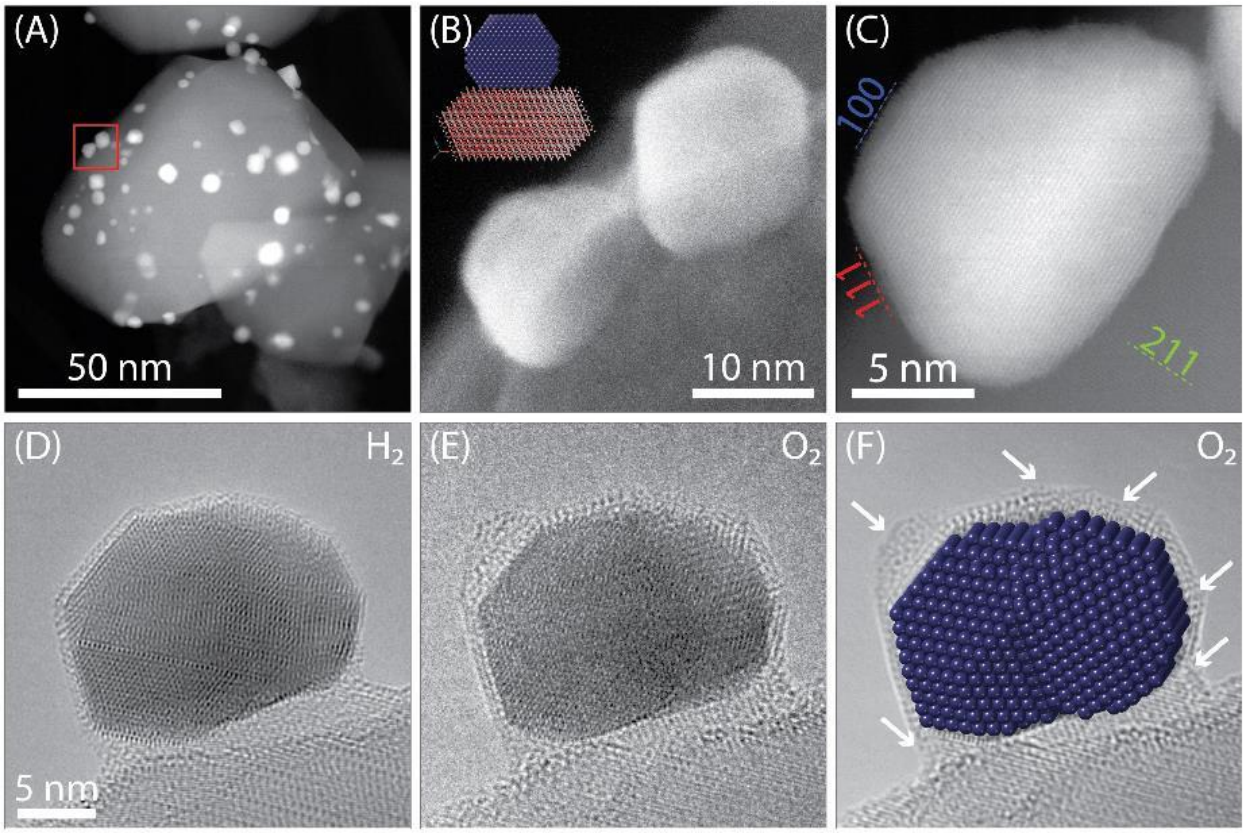

Fig. S1. Starting material and encapsulated Pt NP under H_2 and O_2. A: Annular dark-field (ADF) STEM image of the Pt/TiO_2 catalyst, showing the distribution of small Pt particles on larger TiO_2 support particles. **B:** Secondary electron image of two representative Pt particles that show a low surface wetting and are shaped in the form of truncated cuboctahedra. **C:** ADF STEM image recorded at higher magnification revealing lattice fringes and the orientation of exposed platinum surfaces. **D**: A platinum particle with the classical SMSI overlayer imaged at 600 °C in 700 mbar hydrogen. **E:** The same particle after switching from hydrogen, via He to an O_2 atmosphere (600 °C, p_{O2} = 700 mbar). **F:** Image generated by summing over 30 subsequent frames (starting with **E**), corresponding to an integral recording time of 5s and overlayed with a structural model of platinum (not to scale).

Fig. S2.

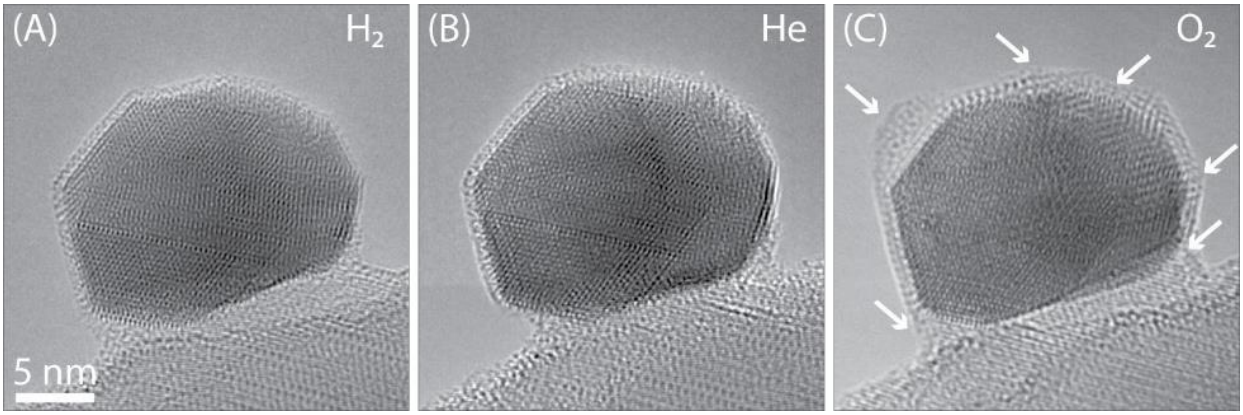

Fig. S2. Platinum-titania at 600 °C under **A**: 1 bar of H_2, **B**: 1 bar of He and **C**: 700 mbar of O_2. Images integrated over 5 seconds exposure time respectively. Arrows in **C** indicate amorphous patches of the overlayer.

Fig. S3.

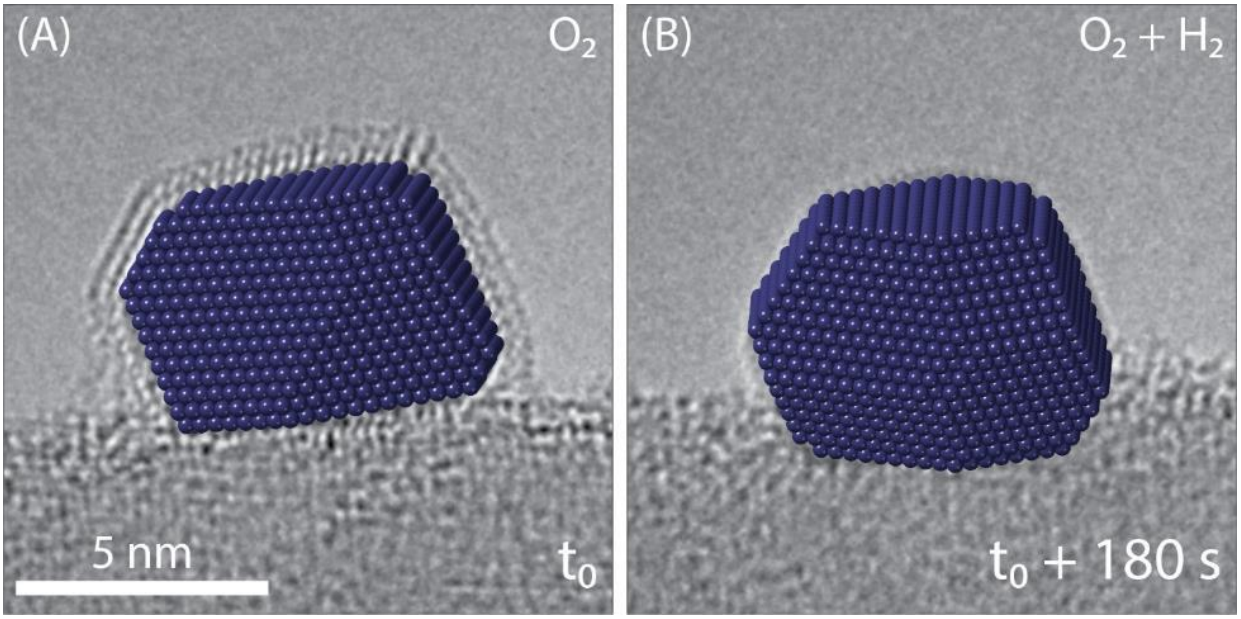

Fig. S3. Pt particle on TiO_2 at 600 °C. (A) under 700 mbar of O_2 and **(B)** under 700 mbar of O_2 and 60 mbar of H_2. The frames shown in **(A)** and **(B)** correspond to **Fig 1 A** and **F** respectively. Superimposed particle models show a change in surface wetting and slight expansion of {100} facets.

Fig. S4.

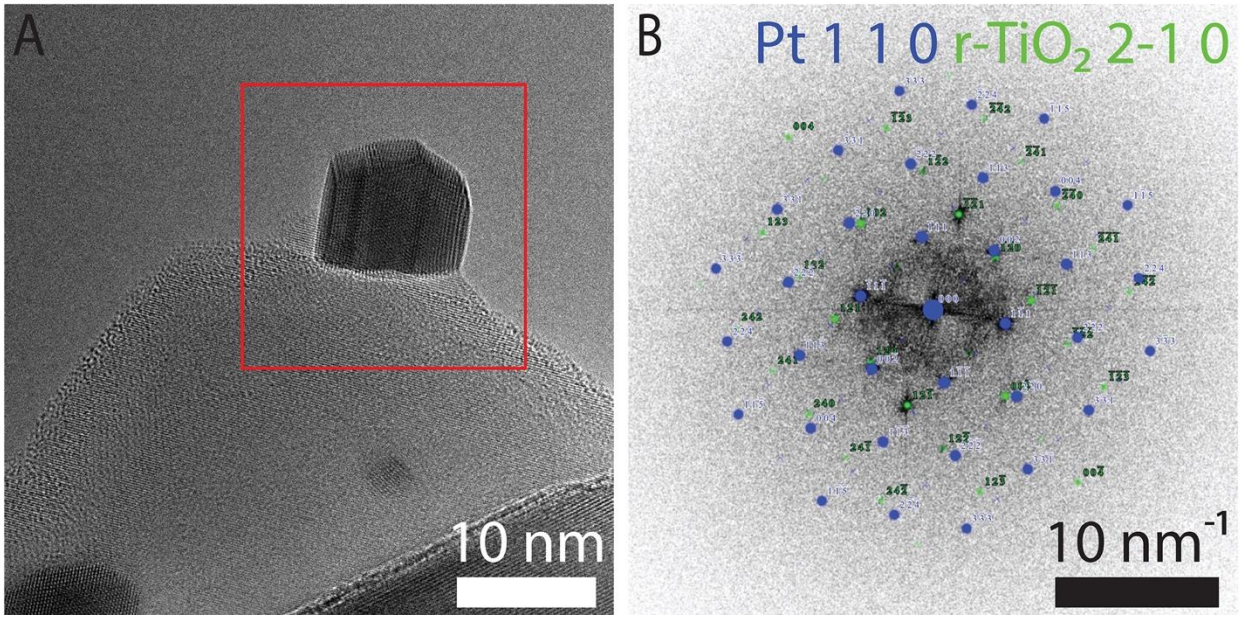

Fig. S4. Fast Fourier Transform (FFT) analysis of ROI in Fig. 3 E. (A) Micrograph shown in **Fig. 3 E**. Red square marks area from where FFT shown in **(B)** was extracted. **(B)** Indexed FFT. Viewing direction for Pt and TiO_2 is shown in legend. Fourier transform in **(B)** shows a proximity in spacing and orientation of Pt {220} and TiO_2 {002} planes and similarly, of Pt {002} and TiO_2 {120} planes, indicating a preferential orientation due to minimization of the lattice misfit induced interfacial strain (*76*).

Fig. S5.

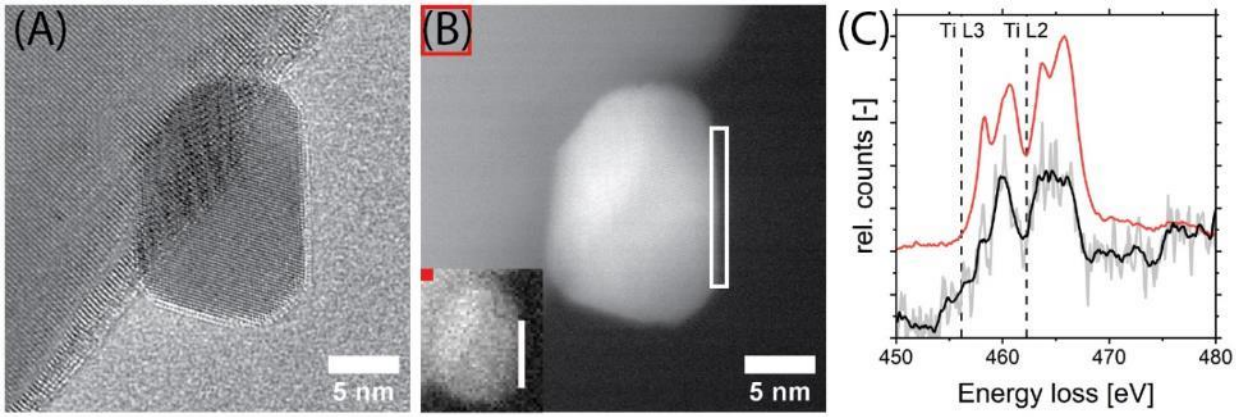

Fig. S5. Pt/TiO_2 at 600 °C and 700 mbar of O_2. (A) HRTEM image of encapsulated platinum particle. **(B)** The same particle imaged with HAADF-STEM. Inset shows the recorded spectral image of the same region. **(C)** Extracted electron energy loss spectra (EELS) from the regions indicated in **(B)** by a red square and a white bar. Ti $L_{3,2}$ edges are clearly visible for both, the support and the particle edge.

Fig. S6.

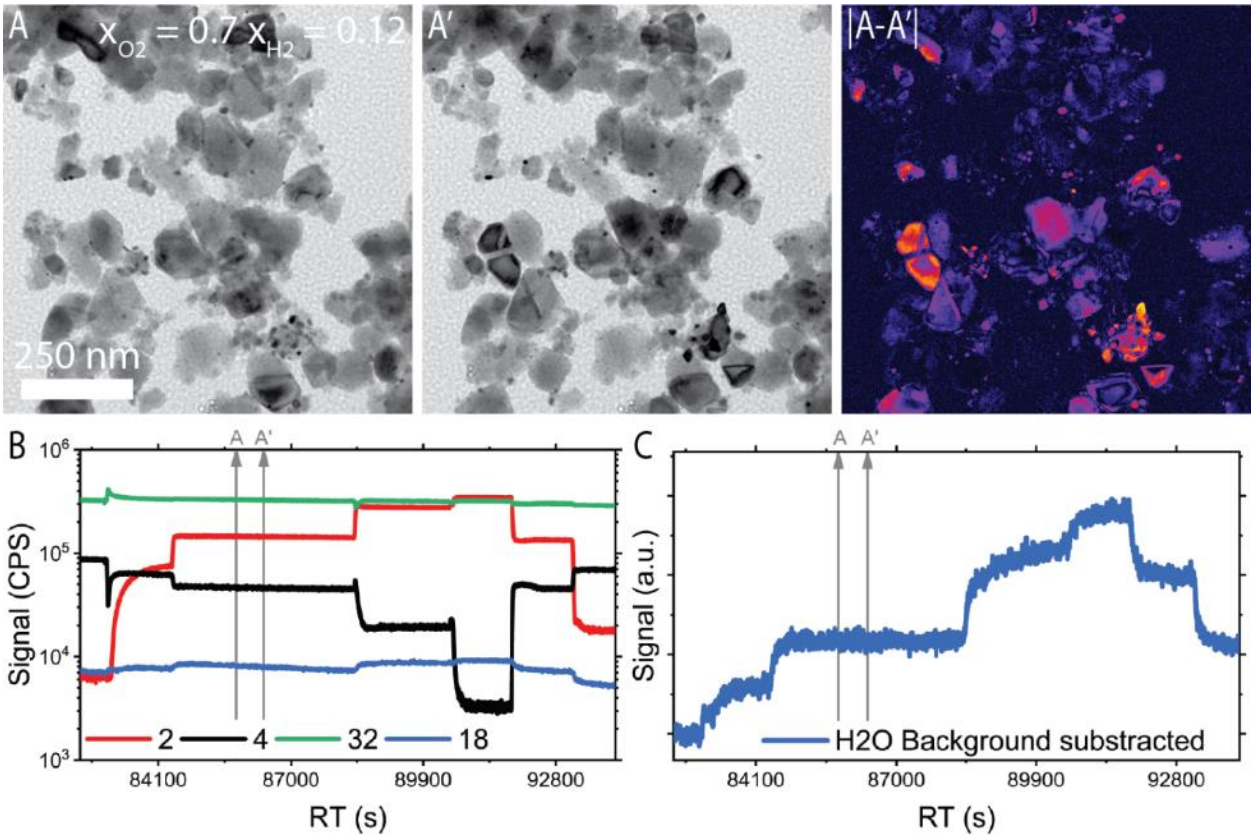

Fig. S6. Mass conversion data. Mass conversion data of the platinum titania catalyst under a constant 700 mbar O_2 pressure and 0, 60, 120, 300, 0 mbar of H_2 at 600°C. **(A)** in situ TEM micrograph of the Pt/TiO_2 sample under 700 mbar of O_2 and 120 mbar of H_2 at 600°C. **(A')**: the same ROI 10 minutes later. |**A-A'**|: Color-coded difference image of **(A)** and **(A')**. Bright areas indicate particle migration. **(B)** Raw MS response, **(C)** Magnified water signal, treated additionally by subtracting a linear background. In **(B)** and **(C)**, the timestamp of **(A)** and **(A')** is indicated by grey arrows.

References and Notes

1. M. Haruta, Size- and support-dependency in the catalysis of gold. *Catal. Today* **36**, 153–166 (1997). doi:10.1016/S0920-5861(96)00208-8

2. T. W. van Deelen, C. Hernández Mejía, K. P. de Jong, Control of metal-support interactions in heterogeneous catalysts to enhance activity and selectivity. *Nat. Catal.* **2**, 955–970 (2019). doi:10.1038/s41929-019-0364-x

3. S. J. Tauster, S. C. Fung, R. L. Garten, Strong metal-support interactions. Group 8 noble metals supported on titanium dioxide. *J. Am. Chem. Soc.* **100**, 170–175 (1978). doi:10.1021/ja00469a029

4. A. Beck, X. Huang, L. Artiglia, M. Zabilskiy, X. Wang, P. Rzepka, D. Palagin, M.-G. Willinger, J. A. van Bokhoven, The dynamics of overlayer formation on catalyst nanoparticles and strong metal-support interaction. *Nat. Commun.* **11**, 3220 (2020). doi:10.1038/s41467-020-17070-2 Medline

5. W. Zhao, D. Zhou, S. Han, Y. Li, J. Liu, Y. Zhou, M. Li, X. Zhang, W. Shen, Metal–Support Interaction in Pt/TiO 2 : Formation of Surface Pt–Ti Alloy. *J. Phys. Chem. C* **125**, 10386–10396 (2021). doi:10.1021/acs.jpcc.1c02108

6. X. Wang, A. Beck, J. A. van Bokhoven, D. Palagin, Thermodynamic insights into strong metal–support interaction of transition metal nanoparticles on titania: Simple descriptors for complex chemistry. *J. Mater. Chem. A Mater. Energy Sustain.* **9**, 4044–4054 (2021). doi:10.1039/D0TA11650E

7. D. N. Belton, Y. M. Sun, J. M. White, Thin-film models of strong metal-support interaction catalysts. Platinum on oxidized titanium. *J. Phys. Chem.* **88**, 1690–1695 (1984). doi:10.1021/j150653a005

8. C. S. Ko, R. J. Gorte, Evidence for diffusion of a partially oxidized titanium species into bulk platinum. *J. Catal.* **90**, 59–64 (1984). doi:10.1016/0021-9517(84)90084-8

9. R. A. Demmin, C. S. Ko, R. J. Gorte, Effect of titania on the chemisorption and reaction properties of platinum. *J. Phys. Chem.* **89**, 1151–1154 (1985). doi:10.1021/j100253a020

10. S. Bernal, F. J. Botana, J. J. Calvino, C. López, J. A. Pérez-Omil, J. M. Rodríguez-Izquierdo, High-resolution electron microscopy investigation of metal–support interactions in Rh/TiO 2. *J. Chem. Soc., Faraday Trans.* **92**, 2799–2809 (1996). doi:10.1039/FT9969202799

11. S. Zhang, P. N. Plessow, J. J. Willis, S. Dai, M. Xu, G. W. Graham, M. Cargnello, F. Abild-Pedersen, X. Pan, Dynamical Observation and Detailed Description of Catalysts under Strong Metal-Support Interaction. *Nano Lett.* **16**, 4528–4534 (2016). doi:10.1021/acs.nanolett.6b01769 Medline

12. J. Lee, S. P. Burt, C. A. Carrero, A. C. Alba-Rubio, I. Ro, B. J. O'Neill, H. J. Kim, D. H. K. Jackson, T. F. Kuech, I. Hermans, J. A. Dumesic, G. W. Huber, Stabilizing cobalt catalysts for aqueous-phase reactions by strong metal-support interaction. *J. Catal.* **330**, 19–27 (2015). doi:10.1016/j.jcat.2015.07.003

13. D. Liu, X. Y. Quek, W. N. E. Cheo, R. Lau, A. Borgna, Y. Yang, MCM-41 supported nickel-based bimetallic catalysts with superior stability during carbon dioxide reforming of

methane: Effect of strong metal-support interaction. *J. Catal.* **266**, 380–390 (2009). doi:10.1016/j.jcat.2009.07.004

14. J. Li, Y. Lin, X. Pan, D. Miao, D. Ding, Y. Cui, J. Dong, X. Bao, Enhanced CO_2 Methanation Activity of Ni/Anatase Catalyst by Tuning Strong Metal–Support Interactions. *ACS Catal.* **9**, 6342–6348 (2019). doi:10.1021/acscatal.9b00401

15. X. Liu, M.-H. Liu, Y.-C. Luo, C.-Y. Mou, S. D. Lin, H. Cheng, J.-M. Chen, J.-F. Lee, T.-S. Lin, Strong metal-support interactions between gold nanoparticles and ZnO nanorods in CO oxidation. *J. Am. Chem. Soc.* **134**, 10251–10258 (2012). doi:10.1021/ja3033235 Medline

16. T. Lunkenbein, J. Schumann, M. Behrens, R. Schlögl, M. G. Willinger, Formation of a ZnO Overlayer in Industrial Cu/ZnO/Al_2O_3 Catalysts Induced by Strong Metal-Support Interactions. *Angew. Chem.* **127**, 4627–4631 (2015). doi:10.1002/ange.201411581

17. H. Tang, Y. Su, Y. Guo, L. Zhang, T. Li, K. Zang, F. Liu, L. Li, J. Luo, B. Qiao, J. Wang, Oxidative strong metal-support interactions (OMSI) of supported platinum-group metal catalysts. *Chem. Sci.* **9**, 6679–6684 (2018). doi:10.1039/C8SC01392F Medline

18. S. Liu, W. Xu, Y. Niu, B. Zhang, L. Zheng, W. Liu, L. Li, J. Wang, Ultrastable Au nanoparticles on titania through an encapsulation strategy under oxidative atmosphere. *Nat. Commun.* **10**, 5790 (2019). doi:10.1038/s41467-019-13755-5 Medline

19. S. Liu, H. Qi, J. Zhou, W. Xu, Y. Niu, B. Zhang, Y. Zhao, W. Liu, Z. Ao, Z. Kuang, L. Li, M. Wang, J. Wang, Encapsulation of Platinum by Titania under an Oxidative Atmosphere: Contrary to Classical Strong Metal–Support Interactions. *ACS Catal.* **11**, 6081–6090 (2021). doi:10.1021/acscatal.1c01347

20. M. Tang, S. Li, S. Chen, Y. Ou, M. Hiroaki, W. Yuan, B. Zhu, H. Yang, Y. Gao, Z. Zhang, Y. Wang, Facet-Dependent Oxidative Strong Metal-Support Interactions of Palladium-TiO_2 Determined by In Situ Transmission Electron Microscopy. *Angew. Chem. Int. Ed.* **60**, 22339–22344 (2021). doi:10.1002/anie.202106805 Medline

21. H. Tang, J. Wei, F. Liu, B. Qiao, X. Pan, L. Li, J. Liu, J. Wang, T. Zhang, Strong Metal-Support Interactions between Gold Nanoparticles and Nonoxides. *J. Am. Chem. Soc.* **138**, 56–59 (2016). doi:10.1021/jacs.5b11306 Medline

22. H. Tang, F. Liu, J. Wei, B. Qiao, K. Zhao, Y. Su, C. Jin, L. Li, J. J. Liu, J. Wang, T. Zhang, Ultrastable Hydroxyapatite/Titanium-Dioxide-Supported Gold Nanocatalyst with Strong Metal-Support Interaction for Carbon Monoxide Oxidation. *Angew. Chem. Int. Ed.* **55**, 10606–10611 (2016). doi:10.1002/anie.201601823 Medline

23. A. K. Datye, M. Votsmeier, Opportunities and challenges in the development of advanced materials for emission control catalysts. *Nat. Mater.* **20**, 1049–1059 (2021). doi:10.1038/s41563-020-00805-3 Medline

24. G. L. Haller, D. E. Resasco, in *Advances in Catalysis* (Elsevier, 1989), vol. 36, pp. 173–235; https://linkinghub.elsevier.com/retrieve/pii/S0360056408600188.

25. A. Corma, P. Serna, P. Concepción, J. J. Calvino, Transforming nonselective into chemoselective metal catalysts for the hydrogenation of substituted nitroaromatics. *J. Am. Chem. Soc.* **130**, 8748–8753 (2008). doi:10.1021/ja800959g Medline

26. J. C. Matsubu, S. Zhang, L. DeRita, N. S. Marinkovic, J. G. Chen, G. W. Graham, X. Pan, P.

Christopher, Adsorbate-mediated strong metal-support interactions in oxide-supported Rh catalysts. *Nat. Chem.* **9**, 120–127 (2017). doi:10.1038/nchem.2607 Medline

27. R. M. Kennedy, L. A. Crosby, K. Ding, C. P. Canlas, A. Gulec, L. D. Marks, J. W. Elam, C. L. Marshall, K. R. Poeppelmeier, P. C. Stair, Replication of SMSI via ALD: TiO2 Overcoats Increase Pt-Catalyzed Acrolein Hydrogenation Selectivity. *Catal. Lett.* **148**, 2223–2232 (2018). doi:10.1007/s10562-018-2458-5

28. M. Macino, A. J. Barnes, S. M. Althahban, R. Qu, E. K. Gibson, D. J. Morgan, S. J. Freakley, N. Dimitratos, C. J. Kiely, X. Gao, A. M. Beale, D. Bethell, Q. He, M. Sankar, G. J. Hutchings, Tuning of catalytic sites in Pt/TiO2 catalysts for the chemoselective hydrogenation of 3-nitrostyrene. *Nat. Catal.* **2**, 873–881 (2019). doi:10.1038/s41929-019-0334-3

29. M. G. Willinger, W. Zhang, O. Bondarchuk, S. Shaikhutdinov, H.-J. Freund, R. Schlögl, A case of strong metal-support interactions: Combining advanced microscopy and model systems to elucidate the atomic structure of interfaces. *Angew. Chem. Int. Ed.* **53**, 5998–6001 (2014). doi:10.1002/anie.201400290 Medline

30. S. Shaikhutdinov, Strong Metal–Support Interaction and Reactivity of Ultrathin Oxide Films. *Catal. Lett.* **148**, 2627–2635 (2018). doi:10.1007/s10562-018-2499-9

31. O. Dulub, W. Hebenstreit, U. Diebold, Imaging cluster surfaces with atomic resolution: The strong metal-support interaction state of Pt supported on TiO2(110). *Phys. Rev. Lett.* **84**, 3646–3649 (2000). doi:10.1103/PhysRevLett.84.3646 Medline

32. P. L. Hansen, J. B. Wagner, S. Helveg, J. R. Rostrup-Nielsen, B. S. Clausen, H. Topsøe, Atom-resolved imaging of dynamic shape changes in supported copper nanocrystals. *Science* **295**, 2053–2055 (2002). doi:10.1126/science.1069325 Medline

33. T. Altantzis, I. Lobato, A. De Backer, A. Béché, Y. Zhang, S. Basak, M. Porcu, Q. Xu, A. Sánchez-Iglesias, L. M. Liz-Marzán, G. Van Tendeloo, S. Van Aert, S. Bals, Three-Dimensional Quantification of the Facet Evolution of Pt Nanoparticles in a Variable Gaseous Environment. *Nano Lett.* **19**, 477–481 (2019). doi:10.1021/acs.nanolett.8b04303 Medline

34. H. Yoshida, K. Matsuura, Y. Kuwauchi, H. Kohno, S. Shimada, M. Haruta, S. Takeda, Temperature-dependent change in shape of platinum nanoparticles supported on CeO2 during catalytic reactions. *Appl. Phys. Express* **4**, 065001 (2011). doi:10.1143/APEX.4.065001

35. Y. Kuwauchi, H. Yoshida, T. Akita, M. Haruta, S. Takeda, Intrinsic catalytic structure of gold nanoparticles supported on TiO2. *Angew. Chem. Int. Ed.* **51**, 7729–7733 (2012). doi:10.1002/anie.201201283 Medline

36. T. W. Hansen, J. B. Wagner, P. L. Hansen, S. Dahl, H. Topsøe, C. J. H. Jacobsen, Atomic-resolution in situ transmission electron microscopy of a promoter of a heterogeneous catalyst. *Science* **294**, 1508–1510 (2001). doi:10.1126/science.1064399 Medline

37. Y. Kuwauchi, S. Takeda, H. Yoshida, K. Sun, M. Haruta, H. Kohno, Stepwise displacement of catalytically active gold nanoparticles on cerium oxide. *Nano Lett.* **13**, 3073–3077 (2013). doi:10.1021/nl400919c Medline

38. Y. Li, M. Kottwitz, J. L. Vincent, M. J. Enright, Z. Liu, L. Zhang, J. Huang, S. D.

Senanayake, W. D. Yang, P. A. Crozier, R. G. Nuzzo, A. I. Frenkel, Dynamic structure of active sites in ceria-supported Pt catalysts for the water gas shift reaction. *Nat. Commun.* **12**, 914 (2021). doi:10.1038/s41467-021-21132-4 Medline

39. J. B. Wagner, F. Cavalca, C. D. Damsgaard, L. D. L. Duchstein, T. W. Hansen, Exploring the environmental transmission electron microscope. *Micron* **43**, 1169–1175 (2012). doi:10.1016/j.micron.2012.02.008 Medline

40. M. Plodinec, H. C. Nerl, R. Farra, M. G. Willinger, E. Stotz, R. Schlögl, T. Lunkenbein, Versatile Homebuilt Gas Feed and Analysis System for *Operando* TEM of Catalysts at Work. *Microsc. Microanal.* **26**, 220–228 (2020). doi:10.1017/S143192762000015X Medline

41. M. Boniface, M. Plodinec, R. Schlögl, T. Lunkenbein, Quo Vadis Micro-Electro-Mechanical Systems for the Study of Heterogeneous Catalysts Inside the Electron Microscope? *Top. Catal.* **63**, 1623–1643 (2020). doi:10.1007/s11244-020-01398-6

42. A. Beck, M. Zabilskiy, M. A. Newton, O. Safonova, M. G. Willinger, J. A. Van Bokhoven, Following the structure of copper-zinc-alumina across the pressure gap in carbon dioxide hydrogenation. *Nat. Catal.* **4**, 488–497 (2021). doi:10.1038/s41929-021-00625-x

43. W. Yuan, B. Zhu, K. Fang, X. Y. Li, T. W. Hansen, Y. Ou, H. Yang, J. B. Wagner, Y. Gao, Y. Wang, Z. Zhang, In situ manipulation of the active Au-TiO_2 interface with atomic precision during CO oxidation. *Science* **371**, 517–521 (2021). doi:10.1126/science.abe3558 Medline

44. J. Vincent, P. Crozier, Atomic-resolution Operando and Time-resolved In Situ TEM Imaging of Oxygen Transfer Reactions Catalyzed by CeO_2-supported Pt Nanoparticles. *Microsc. Microanal.* **26** (S2), 1694–1695 (2020). doi:10.1017/S1431927620018991

45. A. Akram, S. J. Freakley, C. Reece, M. Piccinini, G. Shaw, J. K. Edwards, F. Desmedt, P. Miquel, E. Seuna, D. J. Willock, J. A. Moulijn, G. J. Hutchings, Gas phase stabiliser-free production of hydrogen peroxide using supported gold-palladium catalysts. *Chem. Sci.* **7**, 5833–5837 (2016). doi:10.1039/C6SC01332E Medline

46. M. Chi, C. Wang, Y. Lei, G. Wang, D. Li, K. L. More, A. Lupini, L. F. Allard, N. M. Markovic, V. R. Stamenkovic, Surface faceting and elemental diffusion behaviour at atomic scale for alloy nanoparticles during in situ annealing. *Nat. Commun.* **6**, 8925 (2015). doi:10.1038/ncomms9925 Medline

47. J. Resasco, S. Dai, G. Graham, X. Pan, P. Christopher, Combining In-Situ Transmission Electron Microscopy and Infrared Spectroscopy for Understanding Dynamic and Atomic-Scale Features of Supported Metal Catalysts. *J. Phys. Chem. C* **122**, 25143–25157 (2018). doi:10.1021/acs.jpcc.8b03959

48. X. Du, H. Tang, B. Qiao, Oxidative Strong Metal–Support Interactions. *Catalysts* **11**, 896 (2021). doi:10.3390/catal11080896

49. R. Vanselow, M. Mundschau, Diffusion and adsorption of titanium oxide on platinum as related to strong metal-support interactions. *J. Catal.* **103**, 426–435 (1987). doi:10.1016/0021-9517(87)90134-5

50. X. Xu, Q. Fu, L. Gan, J. Zhu, X. Bao, Interface-Confined FeO_x Adlayers Induced by Metal Support Interaction in Pt/FeO_x Catalysts. *J. Phys. Chem. B* **122**, 984–990 (2018).

doi:10.1021/acs.jpcb.7b07644 Medline

51. U. Diebold, The surface science of titanium dioxide. *Surf. Sci. Rep.* **48**, 53–229 (2003). doi:10.1016/S0167-5729(02)00100-0

52. T. Kandemir, F. Girgsdies, T. C. Hansen, K.-D. Liss, I. Kasatkin, E. L. Kunkes, G. Wowsnick, N. Jacobsen, R. Schlögl, M. Behrens, In situ study of catalytic processes: Neutron diffraction of a methanol synthesis catalyst at industrially relevant pressure. *Angew. Chem. Int. Ed.* **52**, 5166–5170 (2013). doi:10.1002/anie.201209539 Medline

53. A. Beck, H. Frey, M. Becker, L. Artiglia, M. G. Willinger, J. A. van Bokhoven, Influence of Hydrogen Pressure on the Structure of Platinum–Titania Catalysts. *J. Phys. Chem. C* **125**, 22531–22538 (2021). doi:10.1021/acs.jpcc.1c05939

54. J. M. Herrmann, M. Gravelle-Rumeau-Maillot, P. C. Gravelle, A microcalorimetric study of metal-support interaction in the Pt/TiO2 system. *J. Catal.* **104**, 136–146 (1987). doi:10.1016/0021-9517(87)90343-5

55. G. B. Raupp, J. A. Dumesic, Adsorption of carbon monoxide, carbon dioxide, hydrogen, and water on titania surfaces with different oxidation states. *J. Phys. Chem.* **89**, 5240–5246 (1985). doi:10.1021/j100270a024

56. C. Spreafico, W. Karim, Y. Ekinci, J. A. van Bokhoven, J. VandeVondele, Hydrogen Adsorption on Nanosized Platinum and Dynamics of Spillover onto Alumina and Titania. *J. Phys. Chem. C* **121**, 17862–17872 (2017). doi:10.1021/acs.jpcc.7b03733

57. K. Zhang, L. Li, S. Shaikhutdinov, H.-J. J. Freund, Carbon Monoxide Oxidation on Metal-Supported Monolayer Oxide Films: Establishing Which Interface is Active. *Angew. Chem. Int. Ed.* **57**, 1261–1265 (2018). doi:10.1002/anie.201710934 Medline

58. A. J. Fox, B. Drawl, G. R. Fox, B. J. Gibbons, S. Trolier-McKinstry, Control of crystallographic texture and surface morphology of Pt/Tio_2 templates for enhanced PZT thin film texture. *IEEE Trans. Ultrason. Ferroelectr. Freq. Control* **62**, 56–61 (2015). doi:10.1109/TUFFC.2014.006671 Medline

59. P. Müller, R. Kern, Equilibrium nano-shape changes induced by epitaxial stress (generalised Wulf–Kaishew theorem). *Surf. Sci.* **457**, 229–253 (2000). doi:10.1016/S0039-6028(00)00371-X

60. C. Castellarin-Cudia, S. Surnev, G. Schneider, R. Podlucky, M. G. Ramsey, F. P. Netzer, Strain-induced formation of arrays of catalytically active sites at the metal–oxide interface. *Surf. Sci.* **554**, L120–L126 (2004). doi:10.1016/j.susc.2004.01.059

61. A. Ruiz Puigdollers, P. Schlexer, S. Tosoni, G. Pacchioni, Increasing oxide reducibility: The role of metal/oxide interfaces in the formation of oxygen vacancies. *ACS Catal.* **7**, 6493–6513 (2017). doi:10.1021/acscatal.7b01913

62. J. L. Vincent, P. A. Crozier, Operando Insight into Oxygen Transfer at Pt/CeO_2 Interfaces during CO Oxidation. *Microsc. Microanal.* **25** (S2), 1508–1509 (2019). doi:10.1017/S1431927619008274

63. S. C. Ammal, A. Heyden, Modeling the noble metal/TiO2 (110) interface with hybrid DFT functionals: A periodic electrostatic embedded cluster model study. *J. Chem. Phys.* **133**, 164703 (2010). doi:10.1063/1.3497037 Medline

64. C. Bäumer, R. Dittmann, in *Metal Oxide-Based Thin Film Structures* (Elsevier, 2018), pp. 489–522; https://linkinghub.elsevier.com/retrieve/pii/B9780128111666000200.

65. R. J. Kamaladasa, A. A. Sharma, Y.-T. T. Lai, W. Chen, P. A. Salvador, J. A. Bain, M. Skowronski, Y. N. Picard, In situ TEM imaging of defect dynamics under electrical bias in resistive switching rutile-TiO_2. *Microsc. Microanal.* **21**, 140–153 (2015). doi:10.1017/S1431927614013555 Medline

66. D. S. Jeong, H. Schroeder, U. Breuer, R. Waser, Characteristic electroforming behavior in Pt/TiO2/Pt resistive switching cells depending on atmosphere. *J. Appl. Phys.* **104**, 123716 (2008). doi:10.1063/1.3043879

67. L. A. Bursill, B. G. Hyde, On the aggregation of wadsley defects in slightly reduced rutile. *Philos. Mag.* **23**, 3–15 (1971). doi:10.1080/14786437108216361

68. L. A. Bursill, B. G. Hyde, D. K. Philp, New crystallographic shear families derived from the rutile structure, and the possibility of continuous ordered solid solution. *Philos. Mag.* **23**, 1501–1513 (1971). doi:10.1080/14786437108217017

69. B. F. Donovan, D. M. Long, A. Moballegh, N. Creange, E. C. Dickey, P. E. Hopkins, Impact of intrinsic point defect concentration on thermal transport in titanium dioxide. *Acta Mater.* **127**, 491–497 (2017). doi:10.1016/j.actamat.2017.01.018

70. M. D. Rasmussen, L. M. Molina, B. Hammer, Adsorption, diffusion, and dissociation of molecular oxygen at defected TiO2(110): A density functional theory study. *J. Chem. Phys.* **120**, 988–997 (2004). doi:10.1063/1.1631922 Medline

71. P. Liu, T. Wu, J. Madsen, J. Schiøtz, J. B. Wagner, T. W. Hansen, Transformations of supported gold nanoparticles observed by in situ electron microscopy. *Nanoscale* **11**, 11885–11891 (2019). doi:10.1039/C9NR02731A Medline

72. W. Gao, Z. D. Hood, M. Chi, Interfaces in Heterogeneous Catalysts: Advancing Mechanistic Understanding through Atomic-Scale Measurements. *Acc. Chem. Res.* **50**, 787–795 (2017). doi:10.1021/acs.accounts.6b00596 Medline

73. P. Mars, D. W. van Krevelen, Oxidations carried out by means of vanadium oxide catalysts. *Chem. Eng. Sci.* **3**, 41–59 (1954). doi:10.1016/S0009-2509(54)80005-4

74. R. Schaub, P. Thostrup, N. Lopez, E. Laegsgaard, I. Stensgaard, J. K. Nørskov, F. Besenbacher, Oxygen vacancies as active sites for water dissociation on rutile TiO(2)(110). *Phys. Rev. Lett.* **87**, 266104 (2001). doi:10.1103/PhysRevLett.87.266104 Medline

75. F. Pesty, H.-P. Steinrück, T. E. Madey, Thermal stability of Pt films on TiO2(110): Evidence for encapsulation. *Surf. Sci.* **339**, 83–95 (1995). doi:10.1016/0039-6028(95)00605-2

76. A. Wilson, A. Bailly, R. Bernard, Y. Borensztein, A. Coati, B. Croset, H. Cruguel, A. Naitabdi, M. Silly, M.-C. Saint-Lager, A. Vlad, N. Witkowski, Y. Garreau, G. Prevot, Gas-induced selective re-orientation of Au-Cu nanoparticles on TiO_2 (110). *Nanoscale* **11**, 752–761 (2019). doi:10.1039/C8NR07645F Medline